



HAL
open science

Multiple hPOT1–TPP1 cooperatively unfold contiguous telomeric G-quadruplexes proceeding from 3' toward 5', a feature due to a 3'-end binding preference and to structuring of telomeric DNA

Jean Chatain, Georges Hatem, Emmanuelle Delagoutte, Jean-François Riou, Patrizia Alberti, Carole Saintomé

► To cite this version:

Jean Chatain, Georges Hatem, Emmanuelle Delagoutte, Jean-François Riou, Patrizia Alberti, et al.. Multiple hPOT1–TPP1 cooperatively unfold contiguous telomeric G-quadruplexes proceeding from 3' toward 5', a feature due to a 3'-end binding preference and to structuring of telomeric DNA. *Nucleic Acids Research*, 2021, 49, pp.10735 - 10746. 10.1093/nar/gkab768 . mnhn-03383266

HAL Id: mnhn-03383266

<https://mnhn.hal.science/mnhn-03383266>

Submitted on 18 Oct 2021

HAL is a multi-disciplinary open access archive for the deposit and dissemination of scientific research documents, whether they are published or not. The documents may come from teaching and research institutions in France or abroad, or from public or private research centers.

L'archive ouverte pluridisciplinaire **HAL**, est destinée au dépôt et à la diffusion de documents scientifiques de niveau recherche, publiés ou non, émanant des établissements d'enseignement et de recherche français ou étrangers, des laboratoires publics ou privés.

Multiple hPOT1–TPP1 cooperatively unfold contiguous telomeric G-quadruplexes proceeding from 3′ toward 5′, a feature due to a 3′-end binding preference and to structuring of telomeric DNA

Jean Chatain¹, Georges Hatem¹, Emmanuelle Delagoutte¹, Jean-François Riou¹, Patrizia Alberti¹ and Carole Saintomé^{1,2,*}

¹Structure et Instabilité des Génomes, Muséum national d'Histoire naturelle, CNRS, INSERM, 43 rue Cuvier, F-75005 Paris, France and ²Sorbonne Université, UFR927, F-75005 Paris, France

Received October 09, 2020; Revised August 04, 2021; Editorial Decision August 21, 2021; Accepted September 15, 2021

ABSTRACT

Telomeres are DNA repeated sequences that associate with shelterin proteins and protect the ends of eukaryotic chromosomes. Human telomeres are composed of 5′TTAGGG repeats and ends with a 3′ single-stranded tail, called G-overhang, that can be specifically bound by the shelterin protein hPOT1 (human Protection of Telomeres 1). *In vitro* studies have shown that the telomeric G-strand can fold into stable contiguous G-quadruplexes (G4). In the present study we investigated how hPOT1, in complex with its shelterin partner TPP1, binds to telomeric sequences structured into contiguous G4 in potassium solutions. We observed that binding of multiple hPOT1–TPP1 preferentially proceeds from 3′ toward 5′. We explain this directionality in terms of two factors: (i) the preference of hPOT1–TPP1 for the binding site situated at the 3′ end of a telomeric sequence and (ii) the cooperative binding displayed by hPOT1–TPP1 in potassium. By comparing binding in K⁺ and in Li⁺, we demonstrate that this cooperative behaviour does not stem from protein-protein interactions, but from structuring of the telomeric DNA substrate into contiguous G4 in potassium. Our study suggests that POT1-TPP1, in physiological conditions, might preferentially cover the telomeric G-overhang starting from the 3′-end and proceeding toward 5′.

INTRODUCTION

Human telomeres are composed of duplex 5′TTAGGG/3′AATCCC repeats with a 3′ single-stranded

extension named G-overhang (50–300 nt) and six telomeric proteins that constitute the shelterin complex (1). Telomeric DNA can be extended by telomerase, a ribonucleoprotein complex that adds GGTTAG repeats to the G-overhang (2). It has been shown that four human telomeric repeats can fold into a G-quadruplex (G4) (3,4) and that the presence of such a structure can impede the recruitment of telomerase (5–9). Among shelterin proteins, the human telomeric single-stranded DNA binding protein hPOT1 (human Protection of Telomeres 1), involved in chromosome-end protection and in telomere-length regulation (10–15), is able to unfold these structures allowing proper extension by telomerase *in vitro* (5). hPOT1 consists of three OB fold (oligonucleotide/oligosaccharide binding) domains: OB1 and OB2 are involved in DNA binding (16) and OB3 in the interaction with its shelterin partner TPP1 (Figure 1A). It has been shown that hPOT1 is sequence specific (16, 17); the OB1 domain recognizes the 5′-TTAGGG-3′ motif, while the OB2 domain binds the 5′-TTAG-3′ motif (16). Thus, the 10 nt 5′-TTAGGGTTAG-3′ sequence is the minimum binding site of hPOT1. hPOT1 is recruited at telomeres thanks to its interactions with hTPP1 (18–19). hTPP1 also recruits telomerase to telomeres and the heterodimer hPOT1–TPP1 acts as a processivity factor for telomerase activity *in vitro* (20). Although TPP1 contains an N-terminal OB fold (Figure 1A), no binding has ever been observed between DNA and TPP1 alone. The hPOT1–TPP1 complex has a higher binding affinity for DNA than hPOT1 alone (20–21).

Several biochemical and biophysical studies have been undertaken in order to understand the mechanism by which hPOT1 unfolds telomeric G4 structures (8,20–25). These studies have focused on a single G4 formed by four repetitions of the human telomeric motif. However, long human telomeric sequences can form contiguous G4 (26–29) that are likely to occur at the G-overhang made of up to

*To whom correspondence should be addressed. Tel: +33 1 40 79 36 86; Email: carole.saintome@mnhn.fr

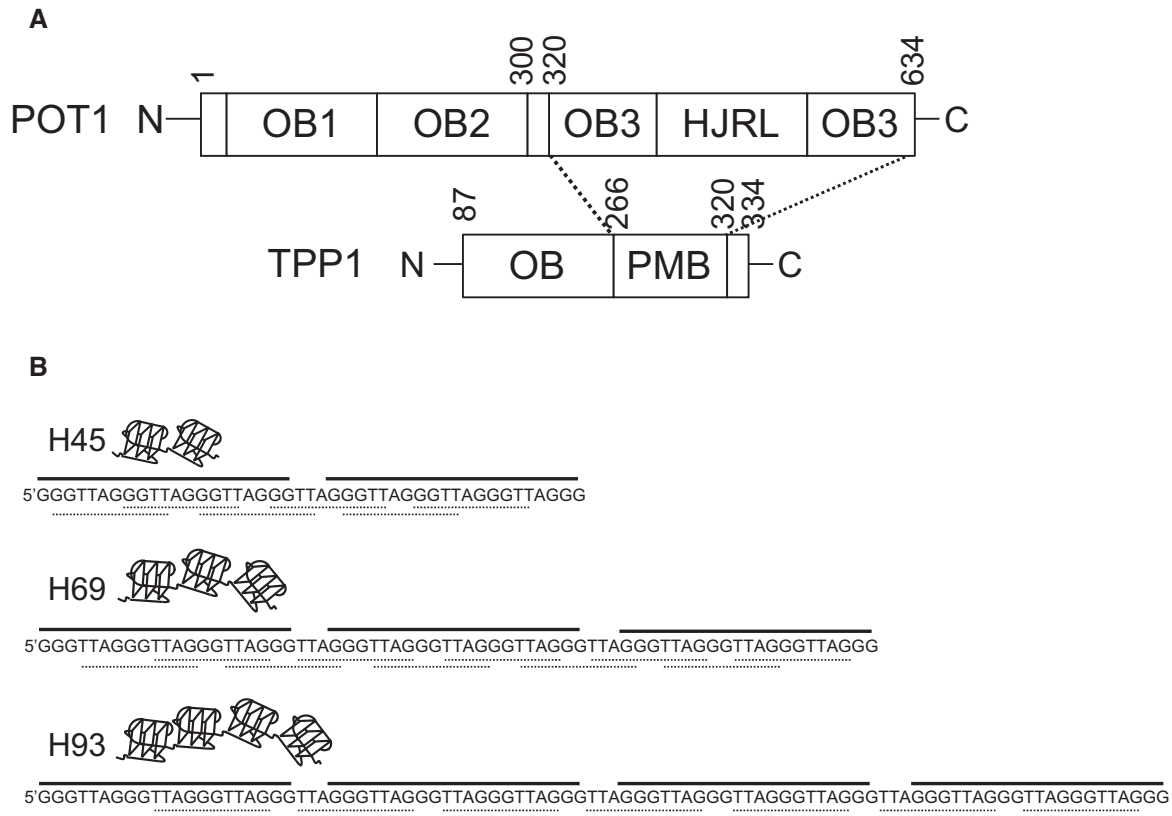


Figure 1. Structure of the human POT1 and TPP1 proteins and telomeric repeat sequences investigated in our study. (A) Domain organization of the hPOT1–TPP1 complex. OB are oligonucleotide/oligosaccharide-binding domains, HJRL is a Holliday junction resolvase-like domain embedded in OB3. TPP1 contains an OB domain and the PBM domain for hPOT1 interaction (indicated by dashed lines); the TBM domain for TIN2 interaction is not present. (B) H45, H69 and H93 are human telomeric sequences; they contain 3, 5 and 7 hPOT1 binding motifs respectively (indicated by dashed lines) and folds into 2, 3 and 4 contiguous G4 (sequences involved in G4 units are indicated by solid lines).

50 tandem repeats. A few studies focused on the interaction of hPOT1 with long human telomeric sequences have shown that multiple hPOT1 fully coat the DNA (30–33). These studies were carried out in the presence of sodium (31,33) or under experimental conditions not promoting the formation of regular contiguous G4 (30) or with sequences forming no more than two contiguous G4 (32). Here, we investigated the interactions of hPOT1–TPP1 with long human telomeric sequences structured into contiguous G4 (up to four G4 units) in the presence of the physiological relevant potassium cations, that stabilize G4 to a larger extent than sodium. Our data reveal that multiple hPOT1–TPP1 feature a 3′-to-5′ directional binding to telomeric sequences folded into stable contiguous G4 and allow explaining the origins of this behaviour.

MATERIALS AND METHODS

Oligonucleotides

Oligonucleotides were purchased from Eurogentec. Non-modified GGGTTA repeats oligonucleotides were PAGE purified, while the double-dye labeled oligonucleotides were RP-HPLC purified by the manufacturer.

The sequences of the double-dye labeled H69-Q1,2,3 oligonucleotides are the following:

H69-Q1: 6FAM-5′(GGGTTA)3GGGTYA(GGGTTA)7GG
 H69-Q2: 5′(GGGTTA)3GGGTXA(GGGTTA)3GGGTYA(GGGTTA)3GGG
 H69-Q3: 5′(GGGTTA)7GGGTXA(GGGTTA)3GGG-TAMRA

where X and Y are 6FAM-dT and TAMRA-dT respectively.

Recombinant proteins preparation

Recombinant hPOT1–TPP1 complex were co-expressed in the baculovirus insect cell system (pFastBac HT-A vector) at the IGBMC-CERBM platform (Strasbourg). The full hPOT1 (residues 1–634) was expressed with six histidines in N-term and a truncated version of human TPP1 (87–334), with a GST-tag in N-term. Each protein contains a restriction site 3C (LGVLFQ/G) that allows removing tags. The cell pellet was resuspended in lysis buffer (50 mM Tris–HCl pH 7.8, 300 mM NaCl, 2 mM DTT, 1 mM PMSF, 2 mM 2-Mercaptoethanol) supplemented with a cocktail of protease inhibitors (Roche), stirred on ice for 1h30. The cells were then lysed by sonication (60% Ampli, 1 s ON–2 s OFF for 20 min) and the cell debris was removed by ultracentrifugation (17 000 rpm for 1h15) at 4°C. The supernatant was loaded on a 5 mL Ni-His Select column pre-equilibrated in

lysis buffer (flow rate 0.15 mL/min). The column was next washed with 25 mL of Ni-Wash buffer (50 mM Tris-HCl pH 7.8, 300 mM NaCl, 2 mM DTT, 10 mM Imidazole) (flow rate 0.5 mL/min, for all the subsequent purification steps). The hPOT1-TPP1 complex was eluted with 25 mL of Ni-Elution buffer (50 mM Tris-HCl pH 7.8, 300 mM NaCl, 2 mM DTT, 300 mM Imidazole). The eluted fractions were loaded on a 5 mL GST column, pre-equilibrated with Ni-Elution Buffer. After a washing step with GST-Wash Buffer (50 mM Tris-HCl pH 7.8, 75 mM NaCl, 1 mM DTT), the hPOT1-TPP1 complex was eluted with GST-Elution Buffer (50 mM Tris-HCl pH 7.8, 300 mM NaCl, 2 mM DTT, and 15 mM GSH). Tags were removed overnight with the PreScission (1500 units) protease at 4°C in Low Salt Buffer (50 mM Tris-HCl pH 7.8, 150 mM NaCl, 1 mM DTT). Finally, the digested sample was loaded on a 1 mL MonoQ column, pre-equilibrated with Low Salt Buffer. The column was next washed with 5 mL of Low Salt Buffer and hPOT1-hTPP1 complex was eluted with a 25 mL gradient of NaCl (from 150 to 300 mM). Fractions containing proteins were pooled and stored at -80°C. Recombinant hRPA was expressed in the *Escherichia coli* BL21 (DE3) strain transformed with the plasmid pET_{11a}hRPA that permits the co-expression of RPA1, RPA2 and RPA3. hRPA was purified as previously described (34).

Electrophoretic mobility shift assays (EMSA)

Oligonucleotides were labeled with γ [³²P]ATP using T4 polynucleotide kinase (NEB). Radiolabeled and doubly-labeled oligonucleotides were heated for 10 min at 85°C and slowly cooled at room temperature. For all EMSA experiments, proteins were diluted and pre-incubated (20 min at 4°C) in a dilution buffer (50 mM Tris-HCl pH 7.5, 100 mM KCl or LiCl, 1 mM DTT, 10% glycerol, 0.2 mg/mL BSA and 0.1 mM EDTA). Oligonucleotides (2 nM for radiolabeled oligonucleotides and 100 nM for double-dye labeled oligonucleotides) were incubated with various amounts of protein in 10 μ L of a reaction buffer (50 mM HEPES pH 7.9, 0.1 mg/mL BSA, 100 mM KCl and 2% glycerol) for 20 min at 20°C. Samples were then loaded on native 5% acrylamide/bisacrylamide (29:1) gels in 0.5X TBE buffer at 4°C. After electrophoresis, gels with radiolabeled oligonucleotides were dried and exposed on a phosphorimager screen, and scanned with a Typhoon instrument (Molecular Dynamics). For double-dye labeled oligonucleotides, gels were directly scanned with Typhoon instrument to detect FAM fluorescence.

Quantification was made with ImageQuant version 5.1. For each protein concentration, the fraction of radiolabeled or doubly-dye labeled oligonucleotides bound to proteins was calculated as follow:

$I_{\text{DNA bound to protein}} / (I_{\text{DNA bound to protein}} + I_{\text{free DNA}})$, where I is the intensity of the band.

Fluorescence resonance energy transfer (FRET)

Fluorescence assays with 100 nM H69-Q1,2,3 oligonucleotides (doubly-labeled with a FAM and a TAMRA) were carried out on a SPEX Fluorolog spectrofluorimeter (Jobin Yvon), in a buffer containing 100 mM KCl and 5 mM acid cacodylic (adjusted at pH 7.2 with LiOH).

For fluorescence titration, the protein (final concentration ranging from 50 to 600 nM) was directly added to the solutions containing the oligonucleotides and incubated for 5 min before recording the emission spectra (excitation wavelength 470 nm). The percentage of opened labeled G4 units at 20°C was calculated as previously described (35).

Fluorescence kinetics experiments were carried out as follows (Supplementary Figure S1): for each double-dye labeled oligonucleotide, the intensity of FAM emission at 518 nm (excitation wavelength 470 nm) was recorded (each 10 s) for 10 min at 20°C ($I_{\text{FAM}}(\text{folded oligo})$), then the protein was added and the intensity of FAM emission was recorded for 40 min ($I_{\text{FAM}}(t)$), finally the temperature was raised to 80°C while continuing to record FAM emission. The intensity of FAM emission of the solution at 80°C provides the intensity of the unfolded oligonucleotides ($I_{\text{FAM}}(\text{unfolded oligo})$). For each kinetics curve, the percentage of unfolded double-dye labeled G4 at the time t after adding the protein was calculated as follows:

$$(I_{\text{FAM}}(t) - I_{\text{FAM}}(\text{folded oligo})) \times 100 / (I_{\text{FAM}}(\text{unfolded oligo}) / 1.15 - I_{\text{FAM}}(\text{folded oligo}))$$

The correction factor 1.15 was applied in order to correct for the slight increase in FAM emission we observed with FAM-labeled telomeric oligonucleotides when increasing the temperature from 20° to 80°C (Supplementary Figure S2). Usually, fluorescent emission decreases with increasing the temperature. The slight increase of FAM emission we observed might be due to the disruption of quenching interactions between FAM and DNA bases when the G4 unfolds at high temperatures. Each experiment was performed two times.

RESULTS

Structuring of telomeric sequences into contiguous G4 affects the binding curve of hPOT1-TPP1

By electrophoretic mobility shift assays (EMSA), we studied the interaction of hPOT1-TPP1 with the following oligonucleotides mimicking human telomeric sequences of increasing length: (GGGTTA)_{7,11,15}GGG, named H45, H69 and H93 respectively. In the presence of potassium, these oligonucleotides fold into two, three and four stable contiguous G4 units, respectively (underlined by bold lines in Figure 1B) (29). Each telomeric sequence contains multiple hPOT1 binding sites: 3 for H45, 5 for H69 and 7 for H93 (TTAGGGTTAG sequences underlined by dashed lines in Figure 1B).

In a standard experiment, 2 nM of radiolabeled DNA was incubated for 20 min at 20°C with different amounts of proteins. Figure 2A shows the results of EMSA. The presence of retarded bands for H45, H69 and H93 indicated that hPOT1-TPP1 binds telomeric DNA in the presence of the physiological relevant cation K⁺, where these sequences are structured into stable contiguous G4. The number of retarded bands increased with the length of the oligonucleotide, revealing hPOT1-TPP1:DNA complexes of increasing stoichiometry, where one, two, three, four, five (or more) hPOT1-TPP1 are bound (Figure 2A). For H45, we observed three retarded bands, indicating the formation of 1:1, 2:1 and 3:1 hPOT1-TPP1:DNA complexes. For H69, we observed five bands, indicating the formation of

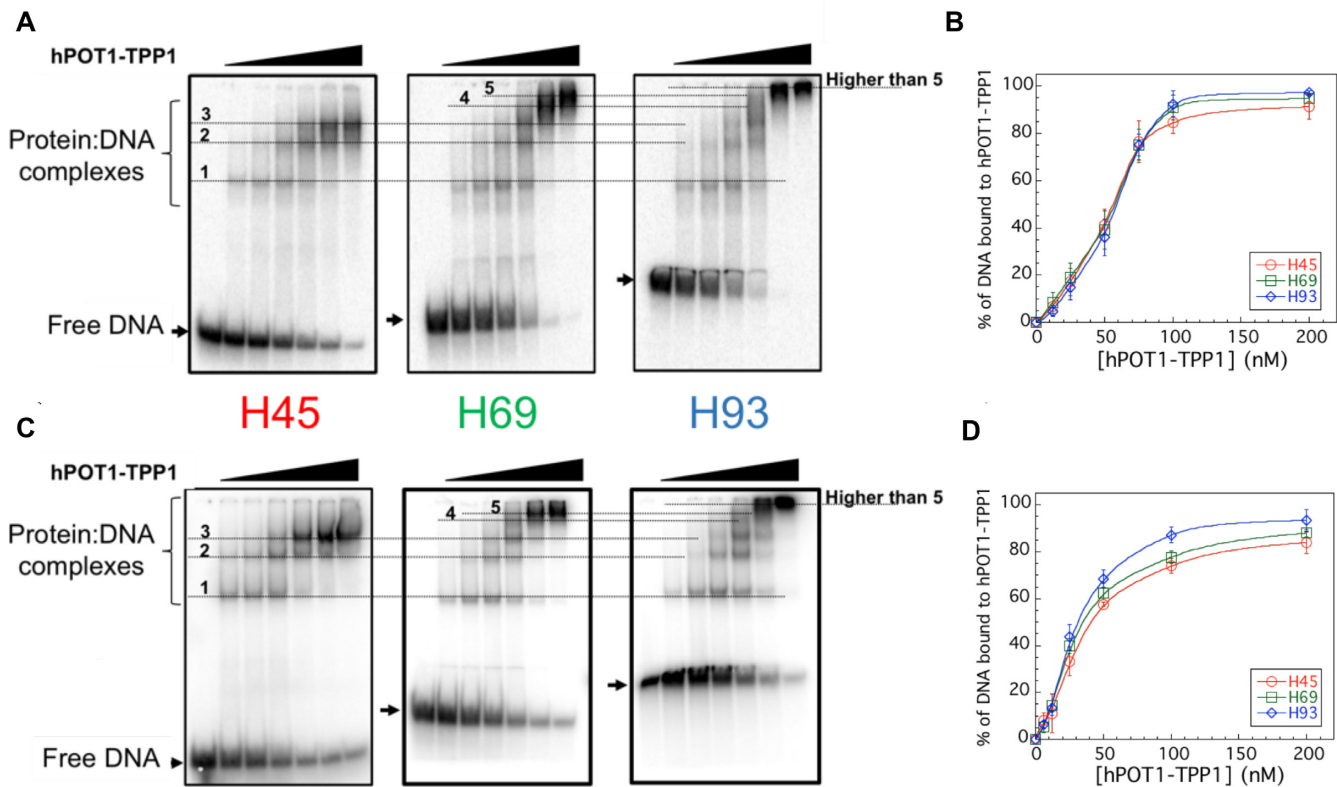


Figure 2. Electrophoretic mobility shift assays. (A, C) EMSA of radiolabeled H45, H69 and H93 oligonucleotides (2 nM) incubated with increasing amounts of hPOT1–TPP1 (0, 12.5, 25, 50, 100 and 200 nM) in 100 mM KCl (A) or LiCl (C). Arrows indicate free DNA; dashed lines indicate protein:DNA complexes of different stoichiometry. (B, D) Percentage of DNA bound to hPOT1–TPP1 as a function of protein concentration in KCl (B) or LiCl (D): H45 (red circles), H69 (green squares) and H93 (blue diamonds). Error bars are standard deviations from three independent experiments.

up to 5:1 hPOT1–TPP1:DNA complexes. The number of retarded bands for H45 and H69, corresponds to the number of hPOT1 binding sites (Figure 1B). For H93, hPOT1–TPP1:DNA complexes with a stoichiometry higher than 5:1 stayed in the well due to their high molecular weight. For the three oligonucleotides, the presence of complexes of intermediate stoichiometry (where not all the binding sites are occupied) indicated that hPOT1–TPP1 does not bind DNA in an ‘all-or-none’ mode. However, quantification of the percentage of DNA bound to hPOT1–TPP1 as a function of concentration resulted in similar sigmoidal curves that suggested a cooperative binding mode (Figure 2B).

A cooperative binding of multiple hPOT1–TPP1 to long telomeric sequences might stem from protein-protein interactions or/and from changes in the DNA substrate upon protein binding. In order to assess whether the sigmoidal shape of the binding curves stemmed from interactions between DNA-bound and free hPOT1–TPP1 complexes or from structuring of DNA into G4, we performed EMSA under ionic conditions where G4 structures were not stabilized, i.e. in the presence of Li⁺ cations (36). Here again, we observed protein:DNA complexes of increasing stoichiometry depending on the length of the DNA (Figure 2C). However, the shape of the binding curves of hPOT1–TPP1 to H45, H69 and H93 oligonucleotides in lithium displayed a less pronounced sigmoidal shape (Figure 2D) (see Supplementary Figure S3A for comparison). Hill plots provided a Hill coefficient of about 2 in KCl and of about 1.3 in LiCl,

suggesting a positive cooperative binding of POT1–TPP1 to telomeric sequences in KCl and a non-cooperative binding in LiCl (Supplementary Figure S3B). Since hPOT1–TPP1 binding to non-structured modified telomeric sequences is not affected by the nature of the monocation (24), our results support that the sigmoidal shape of the binding curves of hPOT1–TPP1 to H45, H69 and H93 in potassium is not due to interactions between free proteins and DNA-bound proteins, but stems from structuring of the DNA substrate into stable contiguous G4 in potassium.

From binding curves in Figures 2B and D, we estimated the apparent binding constants (K_D^{app}). hPOT1–TPP1 displayed a higher K_D^{app} in K⁺ than in Li⁺ (58 ± 2) and (36 ± 5) nM, respectively). A lower affinity in K⁺ than in Li⁺ can be explained by a higher stability of the telomeric G4 in K⁺ than in Li⁺. An inverse correlation between protein affinity and the stability of a single telomeric G4 has already been reported for the first binding event of hPOT1–TPP1 in K⁺ and Na⁺ (24) and for the binding of the single-stranded DNA binding protein RPA in K⁺, Na⁺ and Li⁺ (37).

Unfolding of contiguous G4 by binding of POT1–TPP1 proceeds from 3' toward 5'

It has been shown that POT1 is able to open a single G4 (8,20–25). We wondered whether binding of hPOT1–TPP1 resulted in the unfolding of all contiguous G4s.

To this purpose, classical fluorescence resonance energy transfer (FRET) experiments were carried out on three modified H69 oligonucleotides, doubly-labeled with a 6-carboxyfluorescein (FAM) and a tetramethylrhodamine (TAMRA) at different positions. In H69-Q1 the fluorophores are placed at both sides of the G4 unit at the 5'-end (called 5'-G4 unit, or simply Q1); in H69-Q2 they are placed at both sides of the second G4 unit (called inner-G4 unit, or simply Q2); in H69-Q3 they are placed at both sides of the G4 unit at the 3'-end (called 3'-G4 unit, or simply Q3) (Figure 3) (sequences are detailed in M&M sections) (29,35).

The CD spectra of H69-Q1,2,3 oligonucleotides displayed signatures similar to the one displayed by the non-labeled oligonucleotide H69 (Supplementary Figure S4), suggesting that the double-dye labeling does not dramatically alter, on average, the conformation of the G4 units. Melting profiles of the single double-dye labelled G4 units of these three oligonucleotides were previously recorded by fluorescence (29) and showed that the two external G4 have identical stability (identical melting profiles, with a temperature of half-denaturation $T_{1/2}$ of 60°C), while the inner G4 has a lower stability ($T_{1/2} = 51^\circ\text{C}$) (Supplementary Figure S4). We finally verified that binding of POT1–TPP1 to single-dye labeled telomeric oligonucleotides (coupled with either FAM or TAMRA) quenched neither FAM nor TAMRA fluorescent emission (Supplementary Figure S5). Therefore, any change in FAM and TAMRA emission of H69-Q1,2,3 in the presence of hPOT1–TPP1 can be ascribed to the unwinding of the G4.

For the three H69-Q1,2,3 oligonucleotides, FRET data showed an increase of FAM fluorescence and a decrease in TAMRA fluorescence upon hPOT1–TPP1 addition, indicating that hPOT1–TPP1 unfolds each of the three G4 units (Figure 3A). However, quantification of the opening percentage of the different G4 units showed that at a protein/oligonucleotide ratio r of 1 and 2, the percentage of unfolded 5'-G4 Q1 was very low compared to the percentage of unfolded 3'-G4 Q3 and inner-G4 Q2. The percentage of unfolded 5'-G4 Q1 considerably increased only at $r = 4$ (Figure 3B). It is noteworthy that the opening efficiency of the different G4 units in H69 by hPOT1–TPP1 does not correlate with their stability. Indeed, hPOT1–TPP1 does not open first the less stable G4 (the inner-G4 Q2, characterized by a $T_{1/2}$ of 51°C), and opens the 3'-G4 unit Q3 with a higher efficiency than the 5'-G4 unit Q1, despite their similar stability ($T_{1/2}$ of 60°C). In summary, in titration experiments with the three doubly-labeled H69-Q1,2,3 oligonucleotides, the 5'-G4 unit Q1 is the last to be unfolded.

As a control, we verified that this difference was not due to a difference in protein binding efficiency to the three doubly-labeled H69 oligonucleotides. To this purpose, we carried out EMSA in the same conditions of FRET assays. EMSA experiments showed similar migration patterns (Figure 4) and similar binding efficiency of hPOT1–TPP1 to the three doubly-labeled H69 (see % of bound DNA below the gel in Figure 4A). Indeed, whatever the position of the doubly-labeled G4 in H69, 1 equiv. of hPOT1–TPP1 allowed complexation of 9–10% of DNA with 1 hPOT1–TPP1, 4 equiv. of hPOT1–TPP1 allowed complexation of 55–65% of DNA with up to 3 hPOT1–TPP1, 10 equiv. of hPOT1–TPP1 allowed complexation of all DNA with up

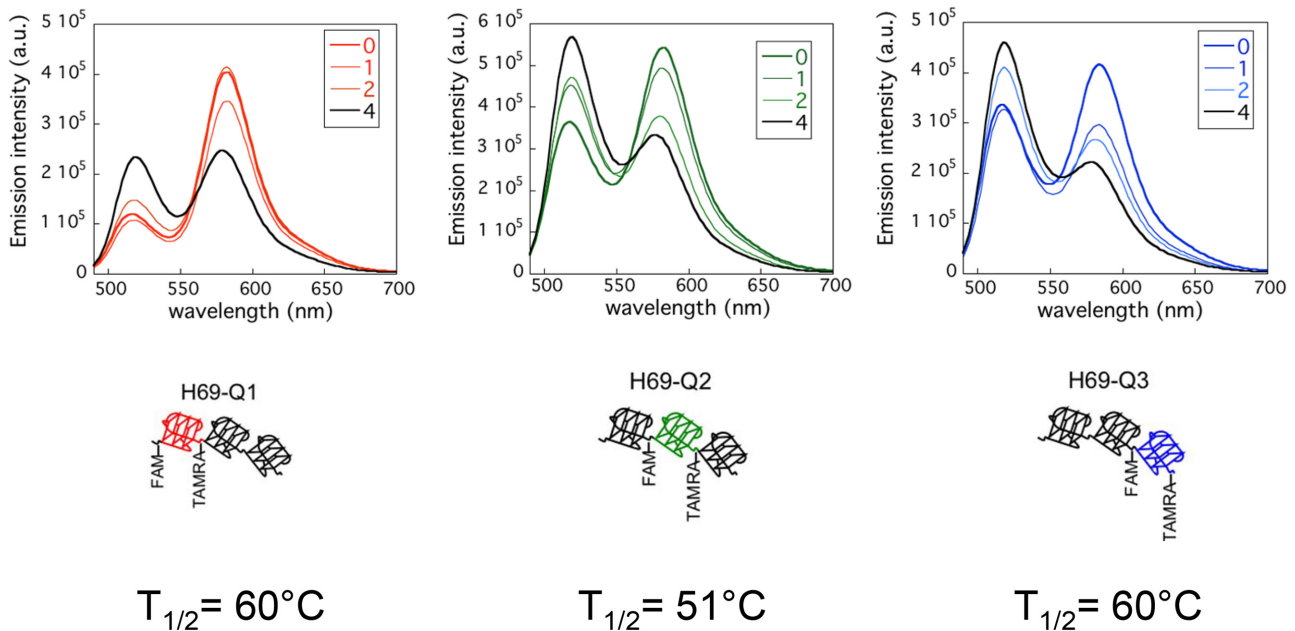
to 5 hPOT1–TPP1. Furthermore, since the binding pattern and efficiency, do not depend on the position of the doubly-labeled G4, we argue that the double-dye labeling does not dramatically alter protein affinities compared to non-labeled oligonucleotides.

We next followed the unfolding kinetics of the doubly-labeled G4 units in H69-Q1,2,3 with 1, 4 and 10 equiv. of hPOT1–TPP1, i.e. under conditions where not all the binding sites are occupied (1 and 4 equiv.) or all the binding sites are occupied (10 equiv.), as indicated by EMSA in the same conditions of FRET assays. From kinetic curves, we calculated the percentage of unfolded G4 units Q1, Q2 and Q3 as a function of time (Figure 5A–C) (as detailed in Materials and Methods) and the percentage of unfolded G4 units at the equilibrium (at the plateau) from two independent experiments (Figure 5D). At 1 equiv. of hPOT1–TPP1, where 1:1 complexes were the major fraction of bound DNA, the 3'-G4 unit Q3 was the one preferentially unfolded ((55 ± 1)%), followed by the inner-G4 unit Q2 ((38 ± 4)%) and by the 5'-G4 unit Q1 ((25 ± 5)%) (Figure 5A and D). At 4 equiv., where 1:1 and 2:1 POT1–TPP1:DNA complexes were the major fractions of bound DNA, a higher percentage of unfolded G4 units was obtained, consistently with the formation of more complexes. However while the 3'-G4 and the inner-G4 units displayed high and similar percentages of unfolding ((78 ± 8)% for Q3 and (69 ± 8)% for Q2), the percentage of unfolded 5'-G4 unit was significantly lower ((35 ± 17)% of unfolded Q1) (Figure 5B and D). At 10 equiv., where 3:1 and 4:1 POT1–TPP1:DNA complexes were the major fractions of bound DNA, similar percentages of unfolded G4 were observed for the three doubly-labeled G4 units (from about 90 to 100% of unfolded Q1, Q2 and Q3) (Figure 5C and D). These results suggest that the binding of multiple hPOT1–TPP1 to H69-Q1,2,3 oligonucleotides proceeds from 3' toward 5'.

To verify that kinetics observed here are POT1–TPP1 specific and not an artefacts due to doubly-labeled oligonucleotides, we carried out kinetics experiments with a different protein. We recently showed that RPA, the eukaryotic single-stranded DNA binding protein, is able to coat long telomeric DNA structured into contiguous G4 (35) and to unfold all the G4. Here, we carried out unfolding kinetics with 6 equiv. of RPA (Figure 5E). Results show that the inner-G4 unit Q2 (which is the less stable) is better unfolded than the two external G4 units Q1 and Q3 (which are more stable). Thus our results with H69-Q1,2,3 suggests that, in a multi-G4 context, hPOT1–TPP1 binding initiates from the 3' end and proceeds towards the 5' end, differently from RPA that binds to G4 structured telomeric sequences starting from the less stable G4 unit.

G4 are polymorphic structures. Different conformations have been resolved for the single G4 formed by the telomeric sequence (GGGTTA)₃GGG in potassium: two hybrid conformation (named hybrid-1 and hybrid-2) and an antiparallel conformation relying on two G-tetrads (named form-3) (38). Like the single telomeric G4 formed by the (GGGTTA)₃GGG core sequence, so also the G4 units in longer telomeric sequences appear to display a certain degree of polymorphism, as suggested by NMR investigations on three contiguous telomeric G4 (39). Might this conformational polymorphism affect the binding patterns

A



B

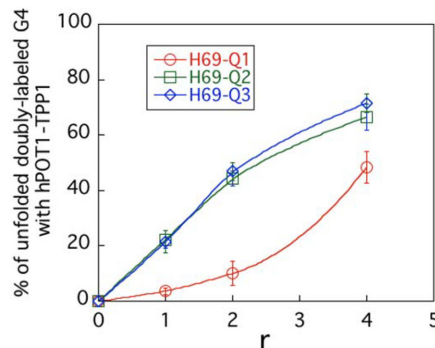


Figure 3. Fluorescence titrations. In order to detect the unfolding of each G4 units, individually, H69 was doubly-labeled with a FAM and a TAMRA at different positions: at the extremities of the G4 at the 5' side (H69-Q1), of the inner G4 (H69-Q2) and of the G4 at the 3' side (H69-Q3). (A) Fluorescence emission spectra (excitation wavelength 470 nm) of H69-Q1, H69-Q2 and H69-Q3 (100 nM) with increasing amounts of hPOT1-TPP1 in 100mM KCl solution, r is the protein/oligonucleotide concentration ratio. Spectra of doubly-labeled oligonucleotides in the absence of protein and in the presence of 4 equiv. of hPOT1-TPP1, are in bold lines. Arrows indicate the evolution of emission spectra with increasing protein concentrations. $T_{1/2}$ is the temperature of half-denaturation of each doubly-labeled G4. (B) Percentage of unfolded labeled G4 units in H69-Q1 (red circles), H69-Q2 (green squares) and H69-Q3 (blue diamonds) as a function of r . The percentage of unfolded labeled G4 units was calculated as previously described (35). Error bars correspond to standard deviations calculated from two independent experiments.

of POT1(-/+TPP1) to a G-overhang? According to a recent study, the unfolding kinetic of hybrid-1 and hybrid-2 G4 conformations by POT1 are identical (25). Nevertheless, a single-molecule study revealed the presence of a minor population that resisted to unfolding by POT1 (23). It will be interesting to undertake single molecule studies on the interaction between POT1(-/+TPP1) and long telomeric sequences structured into contiguous G4 to understand whether this population is present or not in a multimeric-G4 context.

DISCUSSION

Under physiological ionic conditions (in the presence of K^+), long telomeric sequences can fold into stable contiguous G4 (29). Several studies have investigated the binding of the single-stranded DNA binding shelterin POT1 (alone or in complex with its partner TPP1) to telomeric sequences. On one hand, studies in potassium solutions focused on short telomeric sequences folding into a single G4 (8,20–25). On the other hand, studies on longer telomeric sequences were carried out in the presence of sodium (31,33)

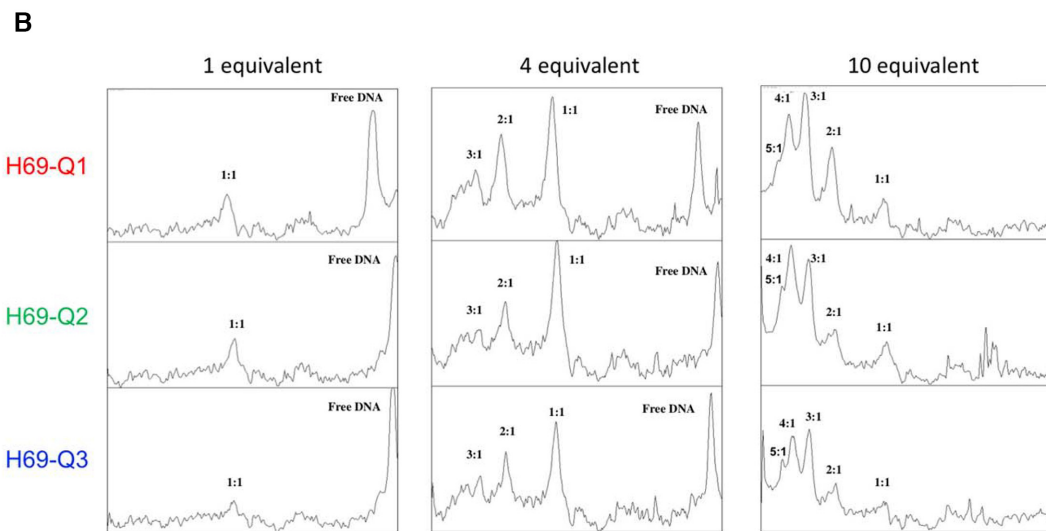
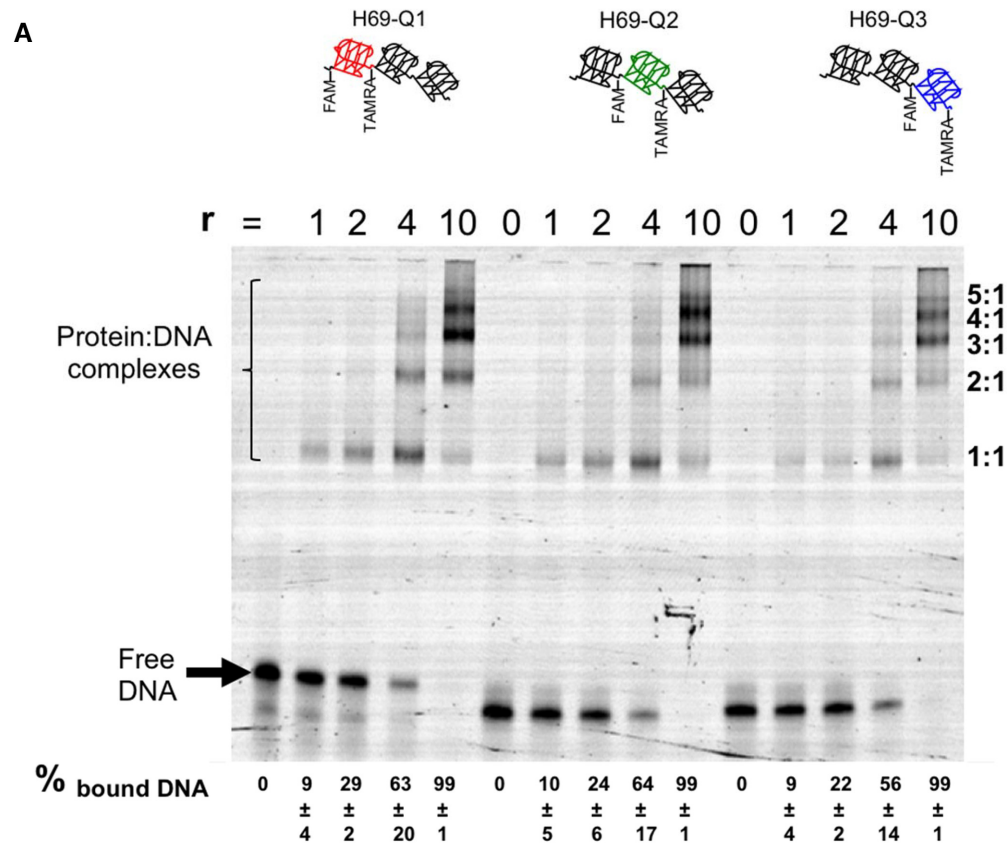


Figure 4. Electrophoretic mobility shift assays in FRET titration conditions. **(A)** EMSA of doubly-labeled H69-Q1,2,3 oligonucleotides (100 nM) incubated with increasing amounts of hPOT1-TPP1 (r is the protein/oligonucleotide concentration ratio) in KCl 100 mM. % of bound DNA (below the gel) was quantified. **(B)** Profiles of EMSA patterns for each lane. 1:1, 2:1, 3:1, 4:1 and 5:1 are the relative intensities of the bands corresponding to hPOT1-TPP1:DNA complexes of increasing stoichiometry.

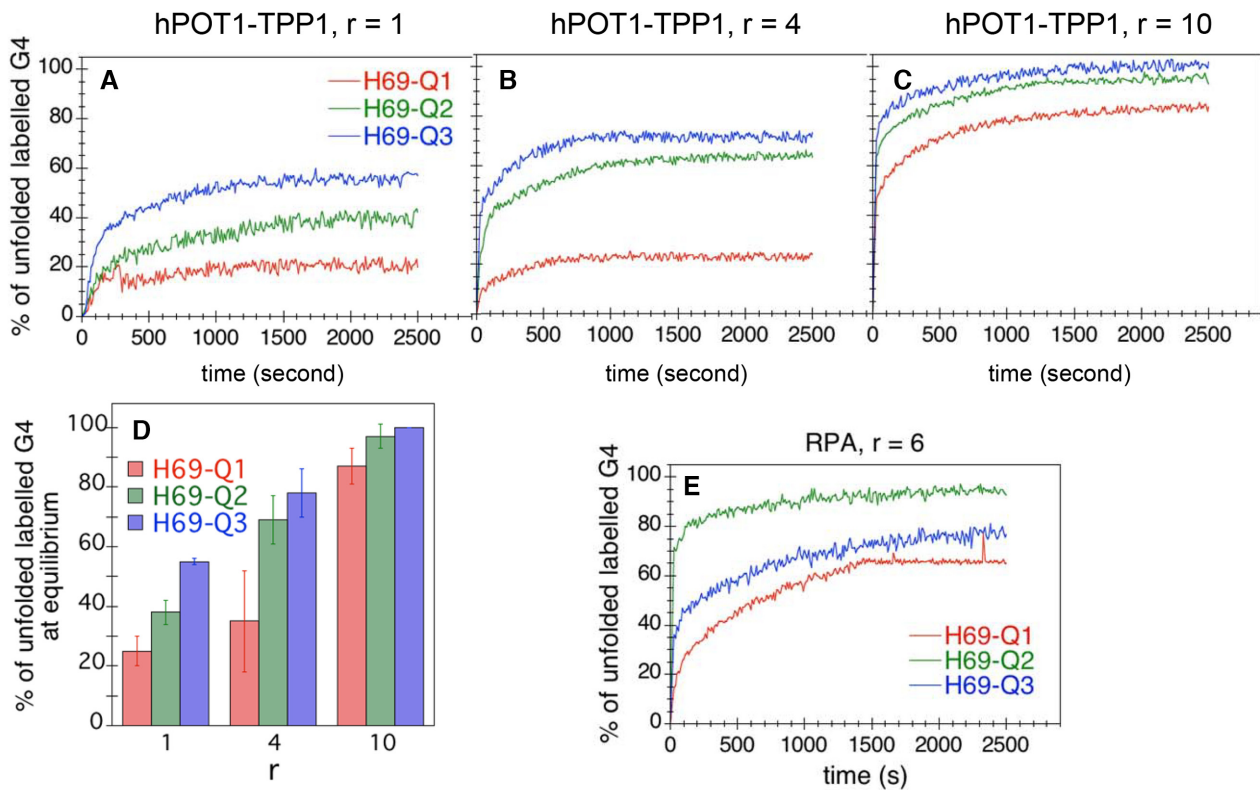


Figure 5. Unfolding Kinetics. Percentage of unfolded doubly-labeled G4 units as a function of time for 100 nM H69-Q1 (red), H69-Q2 (green) and H69-Q3 (blue) with 1 (A), 4 (B) and 10 equiv. (C) of hPOT1-TPP1 and 6 equiv. of hRPA (E), in 100 mM KCl. (D) Percentage of unfolded doubly-labeled G4 units from kinetics curves with hPOT1-TPP1 at equilibrium (plateau). The percentage of unfolded G4 was calculated from fluorescence kinetics as detailed in Materials and Methods section.

or under experimental conditions not promoting the formation of regular contiguous G4 (30) or with sequences forming no more than two contiguous G4 (32). In this work, we investigated how human POT1 in complex with its partner TPP1 copes with stable telomeric contiguous G4 that may form at the telomeric G-overhang. To this purpose, we studied the interaction of hPOT1-TPP1 with oligonucleotides that fold into contiguous G4 in the presence of the biological relevant potassium cation.

We first showed, by EMSA and FRET experiments, that multiple hPOT1-TPP1 bind to long telomeric sequences structured into stable contiguous G4 formed in potassium and form hPOT1-TPP1:DNA complexes where all the binding sites are occupied and all the G4 are unfolded (Figures 2 and 5). When investigating by FRET the unfolding mechanism of three contiguous G4, we observed that at low stoichiometric protein:DNA ratio hPOT1-TPP1 unfolded more efficiently the 3'-G4 unit, at intermediate stoichiometric ratio both the 3'-G4 unit and the inner G4 unit were efficiently unfolded, while the 5'-G4 units was efficiently unfolded only at high stoichiometric ratio (Figure 5D). This support that, in the presence of multiple hPOT1-TPP1, the G4 at the 3' end is the first to be unfolded, followed by the inner G4 and, lastly, by the G4 at the 5' end, revealing a sequential G4 binding/opening mode that proceeds from the G4 at the 3' end toward the G4 at the 5' end.

This directionality did not correlate with the stability of the three G4 units and was specific to hPOT1-TPP1. In-

deed, in our doubly-labeled oligonucleotides H69-Q1,2,3, the 3'-G4 unit was more stable than the inner G4 unit and as stable as the 5'-G4 units (Supplementary Figure S4) and RPA displayed a completely different unfolding pattern, unfolding first the less stable inner G4 unit (Figure 5E). Experiments on a duplex-G4 DNA construct have already suggested that two POT1 bind and unfold the single telomeric G4 formed by the sequence (TTAGGG)₄ in four steps, initiating from the 3'-end and proceeding one OB fold at a time toward 5': first, OB2 binds to the TTAG motif more proximal to the 3' end, then OB1 binds to the TTAGGG motif, followed the sequential binding of OB2 and OB1 of second POT1 (22). Experiments with short DNA sequences (not folding into a G4) where the TTAGGGTTAG binding site is located at the 3' end or at the 5' end show a higher affinity of hPOT1 and hPOT1-TPP1 for the site at the 3' end (Supplementary Figure S7), as previously shown (16,17,20). Such a preference may play a role in the initiation of binding at the 3' end observed for a single G4 (22) and in our multimeric-G4 context. It will be interesting to study whether the 3' end strand of a terminal G4 might also undergo a more pronounced unfolding/folding dynamic, making the binding site at the 3' end more accessible to a first contact by hPOT1(+/-TPP1). Beside a hPOT1(-/+TPP1) 3' end binding preference, there is at least a second factor that makes the unfolding pattern of POT1 and RPA so different with respect to the 3' end. POT1 and RPA display an opposite directionality in their sequential binding to DNA. This may

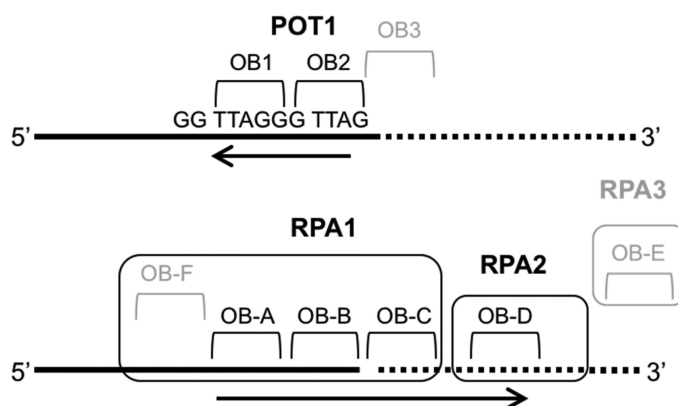


Figure 6. POT1 and RPA binding modes to DNA. POT1 and RPA bind to DNA in an oriented and sequential binding mode (indicated by arrows), involving two OB-fold domains (OB1 and OB2) of POT1 and four OB-fold domains (A–D) of RPA. In POT1, OB2 binds first (to a TTAG motif), followed by OB1 (to a TTAGGG motif) toward 5'. In RPA, OB domains of RPA1 bind first, followed by the OB domain of RPA2 toward 3'. Hence, while a first contact of OB2 to the TTAG motif at the 3' end allows binding of OB1 to achieve the stable 10 nt binding, a first contact of OB domains in RPA1 to a 3' end does not allow achieving the stable 30 nt binding (C).

explain why, contrary to POT1, RPA does not initiate binding at the 3' end. Indeed, while the first contact of a single POT1 to its binding site occurs via the OB2 followed by the binding of OB1 toward 5' (22), the first contact of a single RPA to DNA occurs via its OB domains in the RPA1 subunit followed by the binding of the OB domain in RPA2 subunit toward 3' (40) (Figure 6). Hence, while a first contact of OB2 at the 3' end allows POT1 to achieve its stable 10 nt binding, a first contact of RPA1 to 3' end will not allow to proceed with binding of RPA2 to achieve its stable 30 nt binding and this first contact will likely abort (Figure 6).

As discussed above, a higher affinity and/or accessibility to the site at the 3' end and the 3'-to-5' oriented and sequential binding mode of a single POT1 to DNA (first OB2, followed by OB1) may explain why the binding to G4 structured sequences initiates at the 3' end. Nevertheless, this is not sufficient in itself to explain why the binding proceeds sequentially toward 5' in a multimeric-G4 context as we observed. A second element is necessary to explain this directionality. In EMSA experiments with telomeric sequences folding into up to four contiguous G4, we observed binding curves with sigmoidal shapes in potassium. By comparing the binding of hPOT1–TPP1 in potassium (where the DNA substrate is structured into stable G4) and in lithium (where the DNA substrate does not fold into stable G4), we demonstrated that the sigmoidal shape, displayed only in potassium (Figure 2), does not reflect a cooperativity arising from interactions between DNA-bound and free protein, but mainly stems from structuring of the DNA substrate into stable G4. Sigmoidal binding isotherms have already been observed for the binding of POT1 to a single telomeric G4 in potassium solutions (23, 25). Chaires *et al.* proposed that the sigmoidal shape reflected a conformational selection mechanism, in which binding of POT1 to the telomeric sequence is preceded by unfolding of the G4 (25). We propose that the sigmoidal shape of the binding curve of hPOT1–TPP1 to contiguous G4 in potassium reflects a cooperative binding due to conformational changes of the DNA substrate induced by protein binding. POT1–TPP1 has a

lower affinity for a site embedded in a G4-structured DNA than for a site exposed as a single-strand, as shown by the higher K_D^{app} in LiCl than in KCl, (Figure 2). Each single G4 unit (TTAGGGTTAGGGTTAGGGTTAGGGTTA) in a multimeric-G4 context harbours three potential overlapping POT1 binding sites (TTAGGGTTAG) and four potential binding motifs of the OB2 domain of POT1 (TTAG). In potassium, the binding of a first POT1 to a site embedded into a G4 results in the unfolding of the G4 unit, this makes the other binding sites harboured in the G4 unit exposed as single-strand, thus favoring the binding of a second POT1. This mechanism is consistent with results from a study by Mullins *et al.* on a single telomeric G4, showing that the binding affinity of the first hPOT1–TPP1 binding event is inversely correlated to the stability of the G4 (it is lower in K^+ than in Na^+), while the affinity of the second hPOT1–TPP1 binding event is higher and independent of the nature of the cation (24). We observed a similar cooperativity (arising from the structuring of long telomeric sequences into contiguous G4) also for RPA (35), a protein known to have very little, if any, cooperativity, for unstructured ssDNA (41).

In conclusion, the binding preference of the first hPOT1–TPP1 to the site at the 3' end and the cooperative binding due to the unfolding of the G4 units induced by hPOT1–TPP1 binding, considered together, allow explaining the 3'-to-5' unfolding directionality of contiguous G4 we observed, as illustrated in Figure 7.

We do not exclude the possibility that the first binding event can occur also at an internal site. This may explain why we observed a fraction of unfolded inner G4 and 5'-G4 units even at a protein/DNA ratio of 1 (Figure 5D). However, our results suggest that hPOT1–TPP1 preferentially covers the telomeric G-overhang starting from the 3'-end and proceeding toward 5'. In cells, the majority of the telomeric C-strands end with the sequence CCAATC-5', while the termination of the G-strands is more variable, nevertheless there is a preference for GGTTAG-3', GGGTTA-3' and AGGGTT-3' terminations, with a marked increased preference for GGTTAG-3' termination in cells expressing telom-

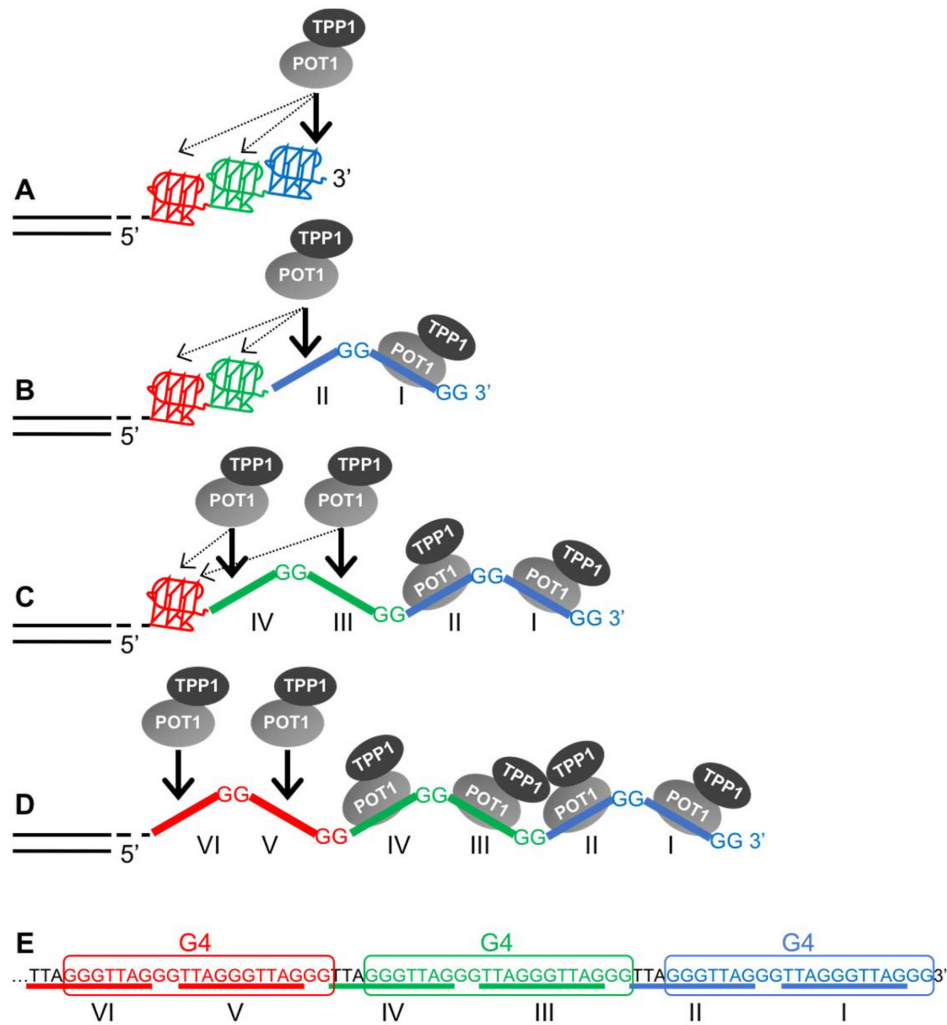


Figure 7. Model of 3'-to-5' directional binding of multiple hPOT1-TPP1 to telomeric sequences structured into contiguous G4. (A) The first binding event occurs at site I, the site at the 3' end, because of a higher accessibility and/or a higher affinity (bold arrow) of hPOT1-TPP1 for this site. (B) Binding of hPOT1-TPP1 to site I results in the unfolding of the G4 at the 3' end (blue G4). Following its unfolding, site II is exposed as a single-strand, thus favoring the binding of a second hPOT1-TPP1. This is because hPOT1-TPP1 has a higher affinity for an unstructured site (bold arrows) than for a site embedded in a G4 (dashed arrows). (C) Binding of a hPOT1-TPP1 to site II destabilizes the second G4 (green G4), favoring the binding of further hPOT1-TPP1 to sites III and IV. (D) This mechanism makes the binding of multiple hPOT1-TPP1 proceed from 3' toward 5'. (E) Telomeric repeats where G4 units are indicated by boxes and hPOT1-TPP1 binding sites by bold lines. This picture holds for G-overhangs with GGG, GGGT, GGGTT or GGGTTA terminations, where the first binding site is embedded in the first G4. GGGTTAG and GGGTTAGG terminations, where the first binding site is partially exposed as a single strand, require a slightly different picture, illustrated in Supplementary Figure S6, that leads to directionality, too.

erase (42) (GGTTAG is the motif added by telomerase). As explained in Supplementary Figure S6, even if the nature of the 3'-end termination of a G-overhang affects the position of POT1-TPP1 binding sites relative to the position of the G4 units, once a first POT1-TPP1 binds to the site at the 3' end, subsequent binding events proceed toward 5', regardless of the nature of the 3'-end termination. Interestingly, the GGTTAG-3' termination (that appears to be the most frequent) leaves the OB2 TTAG binding motif exposed as a single-strand (as shown in Supplementary Figure S6). This may further increase the affinity of hPOT1-TPP1 for the 3' end compared to the internal sites, all embedded into a G4. Binding curves of hPOT1-TPP1 to T10H12 and H12T10 oligonucleotides (where H12 is GGTTAGGGTTAG) show that even at protein/oligo ratio of 50 the 3' binding prefer-

ence is not overcome (100% of bound T10H12 versus less than 40% of bound H12T10) (Supplementary Figure S7). This suggests that hPOT1-TPP1 may feature a preferential 3' to 5' directionality even at elevated hPOT1-TPP1 local concentrations.

In conclusion, our study suggests that hPOT1-TPP1, in physiological conditions, might preferentially cover the telomeric G-overhang starting from the 3' end and proceeding toward 5' end, and allows explaining the origin of this directionality: a preferential binding to the site at the 3' end and a cooperative binding due to the structuring of telomeric sequences into contiguous G4. Our studies on hRPA (40) and the present study reveal peculiar features in the binding of the ssDNA binding proteins hRPA and hPOT1-TPP1 to telomeric sequences structured into G4. On one

side, a single hRPA can bind to internal sequences of the lagging G-strand unfolding G4 from 3' to 5', i.e. in the same direction of the replication fork. On the other hand, multiple hPOT1-TPP1 may preferentially bind to the G-overhang starting from the 3' end and proceeding toward 5'. These different features of RPA and POT1-TPP1 in coping with contiguous telomeric G4 suggest that G4 at telomeres might contribute to modulating the binding of ssDNA binding proteins and their interplay at telomeres (23).

DATA AVAILABILITY

The authors confirm that the data supporting the findings of this study are available within the article and its supplementary data.

SUPPLEMENTARY DATA

Supplementary Data are available at NAR Online.

ACKNOWLEDGEMENTS

We thank the members of the team 'Structure des Acides Nucléiques, Télomères et Evolution' for helpful discussion, Ming Lei for providing hPOT1 and hTPP1 bacmids and Catherine Troffer-Charlier (IGBMC-CERBM platform in Strasbourg) for the baculovirus expression of hPOT1-TPP1.

FUNDING

Muséum national d'Histoire naturelle (MNHN); Centre National de la Recherche Scientifique (CNRS); Institut National de la Santé et de la Recherche Médicale (INSERM); J.C. was supported by a doctoral fellowship from the MNHN Graduate School [ED 227]. Funding for open access charge: CNRS; INSERM.

Conflict of interest statement. None declared.

REFERENCES

- de Lange, T. (2005) Shelterin: The protein complex that shapes and safeguards human telomeres. *Genes Dev.*, **19**, 2100–2110.
- Blackburn, E.H. (2005) Telomeres and telomerase: their mechanisms of action and the effects of altering their functions. *FEBS Lett.*, **579**, 859–862.
- Williamson, J.R. (1994) G-quartet structures in telomeric DNA. *Annu. Rev.*, **23**, 703–730.
- Bryan, T. (2020) G-quadruplexes at telomeres: friend or foe? *Molecules*, **25**, 3686.
- Zaug, A.J., Podell, E.R. and Cech, T.R. (2005) Human POT1 disrupts telomeric G-quadruplexes allowing telomerase extension *in vitro*. *Proc. Natl. Acad. Sci. U.S.A.*, **102**, 10864–10869.
- De Cian, A., Cristofari, G., Reichenbach, P., De Lemos, E., Monchaud, D., Teulade-Fichou, M.P., Shin-Ya, K., Lacroix, L., Lingner, J. and Mergny, J.L. (2007) Reevaluation of telomerase inhibition by quadruplex ligands and their mechanisms of action. *Proc. Natl. Acad. Sci. U.S.A.*, **104**, 17347–17352.
- Wang, Q., Liu, J.Q., Chen, Z., Zheng, K.W., Chen, C.Y., Hao, Y.H. and Tan, Z. (2011) G-quadruplex formation at the 3' end of telomere DNA inhibits its extension by telomerase, polymerase and unwinding by helicase. *Nucleic Acids Res.*, **39**, 6229–6237.
- Hwang, H., Kreig, A., Calvert, J., Lormand, J., Kwon, Y., Daley, J.M., Sung, P., Opresko, P.L. and Myong, S. (2014) Telomeric overhang length determines structural dynamics and accessibility to telomerase and ALT-associated proteins. *Structure*, **22**, 842–853.
- Lee, H.T., Bose, A., Lee, C.Y., Opresko, P.L. and Myong, S. (2017) Molecular mechanisms by which oxidative DNA damage promotes telomerase activity. *Nucleic Acids Res.*, **45**, 11752–11765.
- Baumann, P. (2001) Pot1, the putative telomere end-binding protein in fission yeast and humans. *Science*, **292**, 1171–1175.
- Baumann, P., Podell, E. and Cech, T.R. (2002) Human pot1 (protection of telomeres) protein: Cytolocalization, gene structure, and alternative splicing. *Mol. Cell. Biol.*, **22**, 8079–8087.
- Loayza, D. and de Lange, T. (2003) POT1 as a terminal transducer of TRF1 telomere length control. *Nature*, **423**, 1013–1018.
- Colgin, L.M., Baran, K., Baumann, P., Cech, T.R. and Reddel, R.R. (2003) Human POT1 facilitates telomere elongation by telomerase. *Curr. Biol.*, **13**, 942–946.
- Armbruster, B.N., Linardic, C.M., Veldman, T., Bansal, N.P., Downie, D.L. and Counter, C.M. (2004) Rescue of an hTERT mutant defective in telomere elongation by fusion with hPot1. *Mol. Cell. Biol.*, **24**, 3552–3561.
- Lei, M., Zaug, A.J., Podell, E.R. and Cech, T.R. (2005) Switching human telomerase on and off with hPOT1 protein *in vitro*. *J. Biol. Chem.*, **280**, 20449–20456.
- Lei, M., Podell, E.R. and Cech, T.R. (2004) Structure of human POT1 bound to telomeric single-stranded DNA provides a model for chromosome end-protection. *Nat. Struct. Mol. Biol.*, **11**, 1223–1229.
- Loayza, D., Parsons, H., Donigian, J., Hoke, K. and de Lange, T. (2004) DNA binding features of human POT1. *J. Biol. Chem.*, **279**, 13241–13248.
- Liu, D., Safari, A., O'Connor, M.S., Chan, D.W., Laegeler, A., Qin, J. and Songyang, Z. (2004) PTop interacts with POT1 and regulates its localization to telomeres. *Nat. Cell Biol.*, **6**, 673–680.
- Ye, J.Z.-S., Hockemeyer, D., Krutchinsky, A.N., Loayza, D., Hooper, S.M., Chait, B.T. and de Lange, T. (2004) POT1-interacting protein PIP1: a telomere length regulator that recruits POT1 to the TIN2/TRF1 complex. *Genes Dev.*, **18**, 1649–1654.
- Wang, F., Podell, E.R., Zaug, A.J., Yang, Y., Baciu, P., Cech, T.R. and Lei, M. (2007) The POT1-TPP1 telomere complex is a telomerase processivity factor. *Nature*, **445**, 506–510.
- Xin, H., Liu, D., Wan, M., Safari, A., Kim, H., Sun, W., O'Connor, M.S. and Songyang, Z. (2007) TPP1 is a homologue of ciliate TEBP-beta and interacts with POT1 to recruit telomerase. *Nature*, **445**, 559–562.
- Hwang, H., Buncher, N., Opresko, P.L. and Myong, S. (2012) POT1-TPP1 regulates telomeric overhang structural dynamics. *Structure*, **20**, 1872–1880.
- Ray, S., Bandaria, J.N., Qureshi, M.H., Yildiz, A. and Balci, H. (2014) G-quadruplex formation in telomeres enhances POT1/TPP1 protection against RPA binding. *Proc. Natl. Acad. Sci. USA*, **111**, 2990–2995.
- Mullins, M.R., Rajavel, M., Hernandez-Sanchez, W., de la Fuente, M., Biendarra, S.M., Harris, M.E. and Taylor, D.J. (2016) POT1-TPP1 binding and unfolding of telomere DNA discriminates against structural polymorphism. *J. Mol. Biol.*, **428**, 2695–2708.
- Chaires, J.B., Gray, R.D., Dean, W.L., Monsen, R., DeLeeuw, L.W., Stribinskis, V. and Trent, J.O. (2020) Human POT1 unfolds G-quadruplexes by conformational selection. *Nucleic Acids Res.*, **48**, 4976–4991.
- Yu, H.-Q., Miyoshi, D. and Sugimoto, N. (2006) Characterization of structure and stability of long telomeric DNA G-quadruplexes. *J. Am. Chem. Soc.*, **128**, 15461–15468.
- Xu, Y.K., Loonberg, T. and Komiyama, M. (2009) Human telomeric DNA sequence-specific cleaving by G-quadruplex formation. *J. Am. Chem. Soc.*, **131**, 2871–2874.
- Petraccone, L., Spink, C., Trent, J.O., Garbett, N.C., Mekmaysy, C.S., Giancola, C. and Chaires, J.B. (2011) Structure and stability of higher-order human telomeric quadruplexes. *J. Am. Chem. Soc.*, **133**, 20951–20961.
- Bugaut, A. and Alberti, P. (2015) Understanding the stability of DNA G-quadruplex units in long human telomeric strands. *Biochimie*, **113**, 125–133.
- Wang, H., Nora, G.J., Ghodke, H. and Opresko, P.L. (2010) Single molecule studies of physiologically relevant telomeric tails reveal POT1 mechanism for promoting G-quadruplex unfolding. *J. Biol. Chem.*, **286**, 7479–7489.
- Taylor, D.J., Podell, E.R., Taatjes, D.J. and Cech, T.R. (2011) Multiple POT1-TPP1 proteins coat and compact long telomeric single-stranded DNA. *J. Mol. Biol.*, **410**, 10–17.

32. Corriveau, M., Mullins, M., Baus, D., Harris, M.E. and Taylor, D.J. (2013) Coordinated interactions of multiple POT1-TPP1 proteins with telomere DNA. *J. Biol. Chem.*, **288**, 16361–16370.
33. Xu, M., Kiselar, J., Whited, T.L., Hernandez-Sanchez, W. and Taylor, D.J. (2019) POT1-TPP1 differentially regulates telomerase via POT1 his266 and as a function of single-stranded telomere DNA length. *Proc. Natl. Acad. Sci. U.S.A.*, **116**, 23527–23533.
34. Audry, J., Maestroni, L., Delagoutte, E., Gauthier, T., Nakamura, T.M., Gachet, Y., Saintomé, C., Géli, V. and Coulon, S. (2015) RPA prevents g-rich structure formation at lagging-strand telomeres to allow maintenance of chromosome ends. *EMBO J.*, **34**, 1942–1958.
35. Lancrey, A., Safa, L., Chatain, J., Delagoutte, E., Riou, J.-F., Alberti, P. and Saintomé, C. (2018) The binding efficiency of RPA to telomeric g-strands folded into contiguous g-quadruplexes is independent of the number of G4 units. *Biochimie*, **146**, 68–72.
36. Mergny, J.L. and Lacroix, L. (2009) UV Melting of G-Quadruplexes. *Curr. Protoc. Nucleic Acid Chem.*, **37**, 17.1.1–17.1.15.
37. Safa, L., Delagoutte, E., Petrusseva, I., Alberti, P., Lavrik, O., Riou, J.-F. and Saintomé, C. (2014) Binding polarity of RPA to telomeric sequences and influence of G-quadruplex stability. *Biochimie*, **103**, 80–88.
38. Anh Tuân Phan (2010) Human telomeric G-quadruplex: structures of DNA and RNA sequences. *FEBS Lett.*, **277**, 1107–1117.
39. Hänsel, R., Löhr, F., Trantirek, L. and Dötsch, V. (2013) High-resolution insight into G-overhang architecture. *J. Am. Chem. Soc.*, **135**, 2816–2824.
40. Safa, L., Gueddouda, N.M., Thiébaud, F., Delagoutte, E., Petrusseva, I., Lavrik, O., Mendoza, O., Bourdoncle, A., Laberti, P., Riou, J.F. *et al.* (2016) 5' to 3' unfolding directionality of DNA secondary structures by replication protein A. *J. Biol. Chem.*, **291**, 2146–2156.
41. Kim, C. and Wold, M.S. (1995) Recombinant human replication protein A binds to polynucleotides with low cooperativity. *Biochemistry*, **34**, 2058–2064.
42. Sfeir, A.J., Shay, J.W. and Wright, W.E. (2005) Telomere-end processing the terminal nucleotides of human chromosomes. *Mol. Cell*, **18**, 131–138.